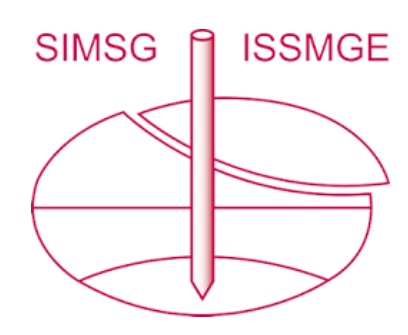
# INTERNATIONAL SOCIETY FOR SOIL MECHANICS AND GEOTECHNICAL ENGINEERING



This paper was downloaded from the Online Library of the International Society for Soil Mechanics and Geotechnical Engineering (ISSMGE). The library is available here:

# https://www.issmge.org/publications/online-library

This is an open-access database that archives thousands of papers published under the Auspices of the ISSMGE and maintained by the Innovation and Development Committee of ISSMGE.

The paper was published in the proceedings of the 10<sup>th</sup> European Conference on Numerical Methods in Geotechnical Engineering and was edited by Lidija Zdravkovic, Stavroula Kontoe, Aikaterini Tsiampousi and David Taborda. The conference was held from June 26<sup>th</sup> to June 28<sup>th</sup> 2023 at the Imperial College London, United Kingdom.

# Proceedings 10th NUMGE 2023

10th European Conference on Numerical Methods in Geotechnical Engineering Zdravkovic L, Kontoe S, Taborda DMG, Tsiampousi A (eds)

© Authors: All rights reserved, 2023 https://doi.org/10.53243/NUMGE2023-247

# DEM investigation of the performance of a bio-inspired selfburrowing probe in granular soils of varying gravity

Bowen Wang<sup>1</sup>, Ningning Zhang<sup>1</sup>, Raul Fuentes<sup>1</sup>, Yuyan Chen<sup>2</sup>, Alejandro Martinez<sup>2</sup>

<sup>1</sup> Institute of Geomechanics and Underground Technology, RWTH Aachen University, Germany <sup>2</sup> Department of Civil and Environmental Engineering, University of California Davis, United States

**ABSTRACT:** In recent years, researchers have attempted to develop self-burrowing probes for soil sensing in locations with limited access such as space exploration and underneath existing structures. The development of the probes is inspired by strategies such as the dual-anchor burrowing of razor clams which cyclically alternates penetrating the back (bivalve shell) and front (pedal or foot) anchors to achieve movement. Using the discrete element method (DEM), we have developed a self-burrowing probe that employs the dual-anchor mechanism (i.e., shaft and tip anchors) and a tip oscillation strategy to achieve effective penetration in granular materials. We investigate the effects of different gravity conditions (i.e., Lunar and Martian gravity) on the performance of the self-burrowing probe, specifically in terms of penetration distance and energy consumption. Results show that in low gravity conditions, the probes are still able to facilitate penetration. The findings in this study may be significant to the potential use of the probe in campaigns of soil testing and sensor deployment on outer-space bodies such as Mars and the Moon.

Keywords: bio-inspired self-burrowing; discrete element method; granular materials; gravity effects

# 1 INTRODUCTION

In recent years, many researchers have been inspired by burrowing natures to develop a variety of self-burrowing robots for subterranean exploration (Dorgan, 2015; Zhang et al., 2019; Wei et al., 2021). According to the bio-burrowing strategies and mechanisms, the main categories include wriggling, undulating, dual-anchoring, grabbing-pushing, reciprocating, granular fluidizing, and root growth. Among these burrowing methods, the dual-anchoring system (Germann et al.,2011; Trueman, 1967) is getting more and more popular because of its simplicity and efficiency (Winter, 2014). Using the discrete element method (DEM) tool, our group has developed a self-burrowing probe with dual-anchoring system (Zhang et al., 2023) and the probe can satisfactorily penetrate a certain depth by repeating burrowing cycles.

Traditional methods for soil investigation in other out-space bodies is drilling, such as Apollo in the moon. In this case, heavy equipment will be sent to the moon which is not convenient and economical and hard to control (Mahaffy et al., 2012). Compared with drilling robots, the self-burrowing robot is lighter and more flexible (Huang & Tao, 2020). While soils in other out-space bodies are different with those on Earth in many aspects due to low gravity effect, it is interesting to explore whether the self-burrowing probe developed under Earthian gravity condtion can still be used in low gravity.

The structure of this paper is organized as follows: First, a brief introduction to the self-burrowing probe is provided. Then, the self-burrowing probe is carried out in soils with relatively low gravity conditions. The self-burrowing perforce and energy consumption are evaluated. All the simulations are performed using the DEM code PFC3D (Itasca, 2017).

# 2 SIMULATIONS OF SELF-BURROWING IN GRANULAR SOILS

# 2.1 Model construction: soil and probe

In this study, particles mimicking the mechanical properties of Fontainebleau sand were filled into a cylindrical chamber to create a shallow and dense soil sample for self-burrowing explorations. Particle diameters ranged from 0.1 to 0.4 mm matching the particle size distribution of Fontainebleau NE34 sand in Figure 1(a). To generate a manageable number of particles and ensure sufficient contacts with the probe, we upscaled the particle sizes with five distinct scaling factors ( $n_1$ =35,  $n_2=53$ ,  $n_3=79$ ,  $n_4=95$ , and  $n_5=113$ ) following the particle refinement method (PRM) (Figure 1b). The contact model parameters (Table 1) were successfully calibrated against element tests using a rough contact model, as reported in Zhang et al. (2021). After filling the particles into the chamber, the soil mass was settled to equilibrium under the gravity level of

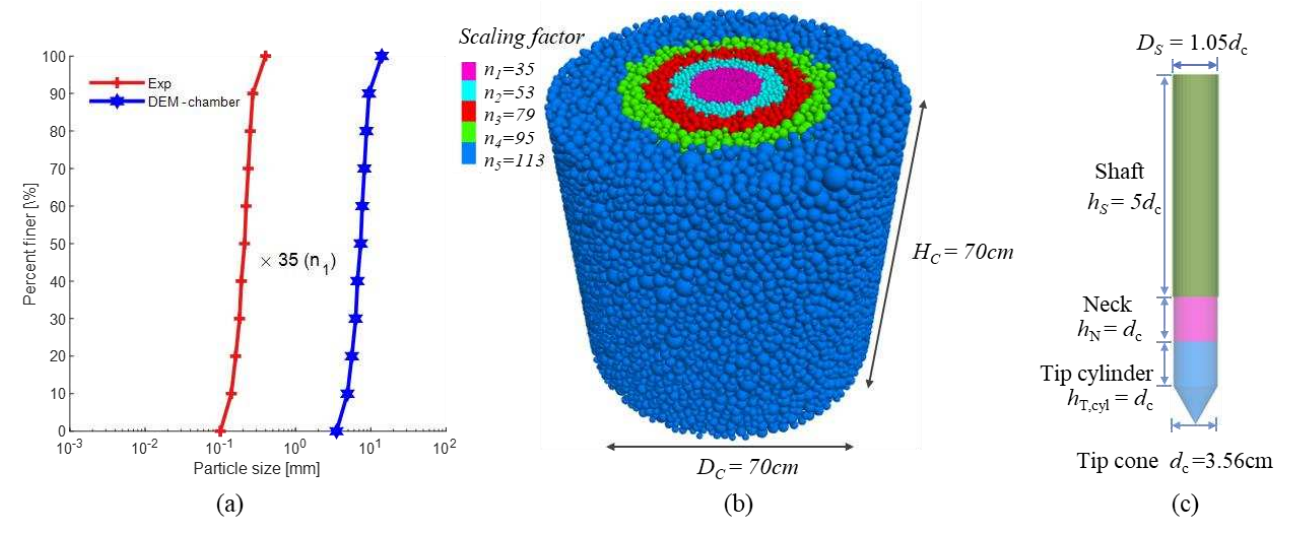


Figure 1. (a) Particle size distribution of Fontainebleau sand, (b) view of soil chamber with multi-scaled particles, and (c) geometry of bio-inspired dual-anchor probe

Table 1. DEM contact model parameters

Element	G (GPa)	v	μ	$S_q$ ( $\mu$ m)	$n_1$	$n_2$
F-sand	2.5	0.19	0.275	0.6	0.05	5
Probe	3.75	0.265	0.35	-	-	-

Note: G, shear modulus; v, Poission's ratio;  $\mu$ , friction coefficient;  $S_q$ , surface roughness;  $n_1$  and  $n_2$ , model parameters.

1/6g, 1/3g, and 1g, respectively, to mimic the gravity conditions on the Moon, Mars and Earth.

Inspired by razor clam locomotion strategies, we created a dual-anchor probe for self-burrowing simulations. Figure 1(c) shows the configuration and geometry of the self-burrowing probe. The probe includes three parts: shaft, neck, and tip. The shaft can expand to provide anchorage force for probe advancement in soils. The tip contains a cylinder that can expand to form another anchor and a cone with an apex angle of 60°. The neck is embedded in the shaft and can move vertically when penetrating.

# 2.2 Self-burrowing procedure

The probe was inserted initially with a constant rate into the three samples with different gravity to explore the feasibility of self-burrowing of the developed probe on relevant outer-space bodies. After reaching a depth of 34 cm, where the probe was fully embedded in the soil, the probe launched its self-burrowing algorithm to autonomously penetrate further into the soil. As depicted in Figure 2, one self-burrowing cycle is completed in six individual steps as follows:

I. Shaft Expansion (SE): To deploy the shaft anchor, the shaft expands radially under constant load control to reach a target force  $F_{S,r,target}$ . A load control

algorithm allows realistic interaction between the probe and soil. The expansion aims to provide sufficient reaction force for tip penetration in step II.

II. Tip Penetration with Oscillation (TPO): With the reaction of the shaft anchor, the neck and tip move downwards for a distance of  $\Delta \rho_{tip}$ . During the downward movement, the tip also oscillates to effectively reduce tip resistance and the shaft target force  $F_{S,r,target}$  is maintained constant to facilitate penetration. This step is terminated as long as one of the following three criteria is triggered: 1) the maximum sliding anchorage force ( $F_{S,r}*\mu$ ) is smaller than the total tip penetration resistance  $Q_T$  (Figure 2); 2) the penetration distance exceeds the cone diameter; and 3) the shaft expansion ratio is greater than 50%.

III. Tip Expansion (TE): The tip cylinder expands to form the bottom anchor using a load control algorithm. The conical portion of the tip is not expanded to avoid interactions with the shaft anchor. The expansion aims to achieve a given target radial force.

IV. Shaft Contraction (SC): The shaft contracts to its original diameter at a constant rate of 0.1 m/s. During the contraction and following shaft retraction, the tip target force reached in TE is maintained constant.

V. Shaft Retraction (SR): The shaft is dragged downwards at a constant rate until the shaft penetration distance  $\Delta \rho_{shaft}$  is equal to  $\Delta \rho_{tip}$ . At this point, the original probe length returns to its original value. This stage is performed under the condition that the anchorage force of the tip is greater than the shaft retraction resistance.

VI. Tip Contraction (TC): The tip contracts back to its original size at a constant rate of 0.1 m.

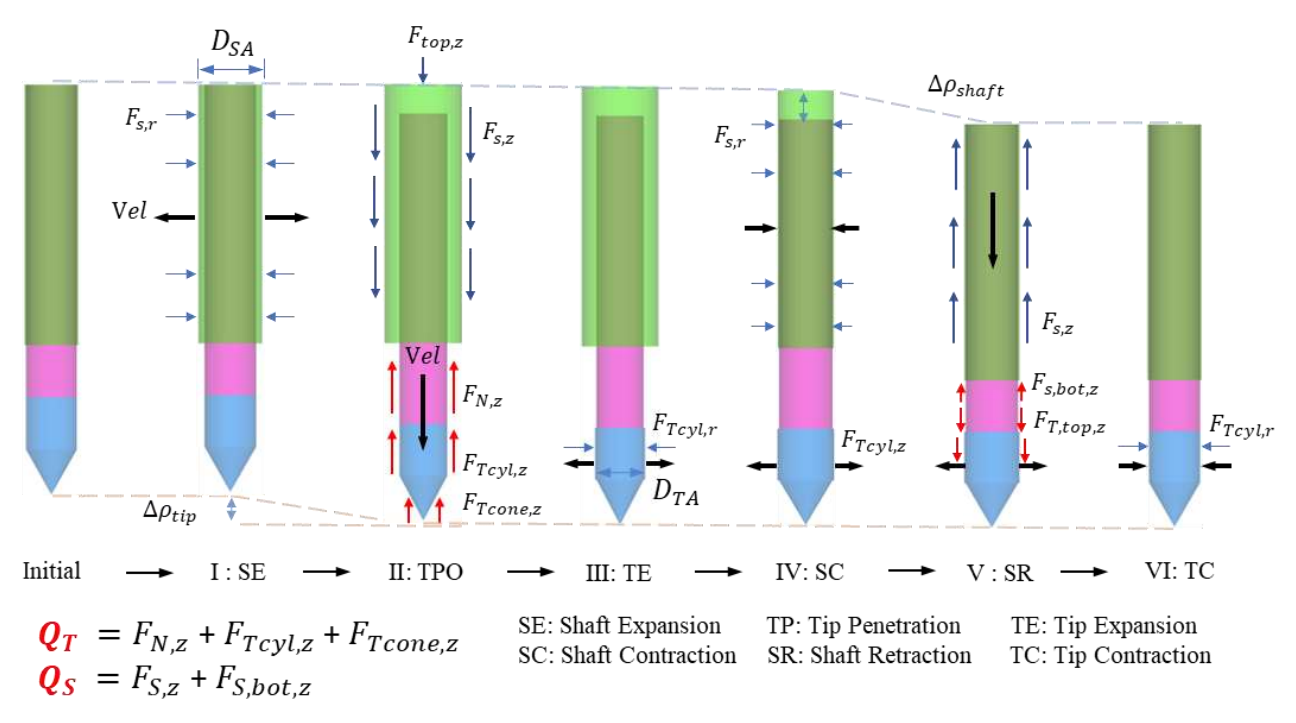


Figure 2. Schematic illustration of a self-burrowing cycle. Thick black arrows represent the movement direction of specific component. Light arrows indicate the direction of forces.

# 3 GRAVITY EFFECTS ON SELF-BURROWING

# 3.1 Penetration forces recorded during initial penetration

During the initial penetration, two resisting force items are recorded:  $Q_T$ , which is the sum of the vertical forces measured along the neck, tip cylinder and tip cone and  $Q_S$ , which is the vertical force measured along the shaft and at the bottom of the shaft (Figure 2). Figure 3 and Figure 4 present the evolution of  $Q_T$  and  $Q_S$  against penetration depth. In all the gravity conditions,  $Q_T$  and  $Q_S$  both increase almost linearly with depth.  $Q_T$  increases with gravity, which agrees with the general observations reported in Jiang et al. (2015). After the probe reached the target depth, a servo control algorithm was initiated to adjust the probe's position to attain an equilibrium state between the probe self-weight and contact forces with surrounding particles.

# 3.2 Characteristic observations during one selfburrowing cycle

The self-burrowing steps described in section 2.2 were run through after the initial penetration stage. Figure 5 shows the evolution of three representative forces recorded on probe segments  $Q_T$ ,  $F_{S,r}$ , and  $F_{Tcyl,r}$  (radial force at the expanded tip) during the whole self-burrowing cycle under the three gravity conditions. In general, the calculation steps are less in high gravity. Concretely in some burrowing steps, primary observations are:

- SE:  $F_{S,r,target}$  increases with gravity, i.e., 0.264 kN for 1/6g, 0.616 kN for 1/3g, and 1.6 kN for 1g.
- TPO and SE: respective force criteria can all be met, indicating the sufficiency of the dual-anchor system.
- TE:  $F_{S,r}$  decreases dramatically. The decrease is sharper with low gravity.

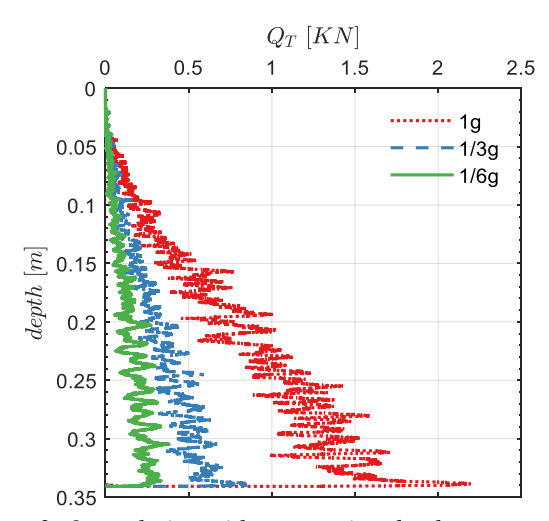


Figure 3.  $Q_T$  evolution with penetration depth.

Tip penetration was all terminated when the criterion of 50% expansion ratio was triggered. Figure 6 shows the evolution of shaft expansion ratio against penetration depth, reflecting self-burrowing performance in the TPO stage. As stated previously, during TPO the shaft keeps expanding to maintain the target force  $F_{S,r,target}$  achieved in the first SE step. It is interesting that under all the simulated gravity conditions, the shaft expansion ratio increases with

similar rates, leading to an equal final penetration depth of 2 cm. This results indicates independency of penetration depth on the gravity conditions, even the values of  $F_{S,r,target}$  are greatly different.

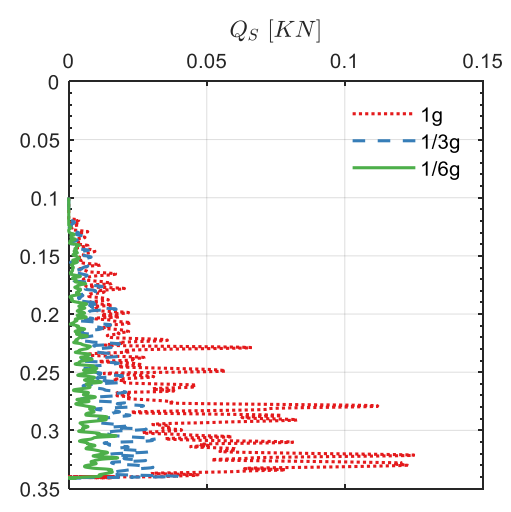


Figure 4. QS evolution with penetration depth.

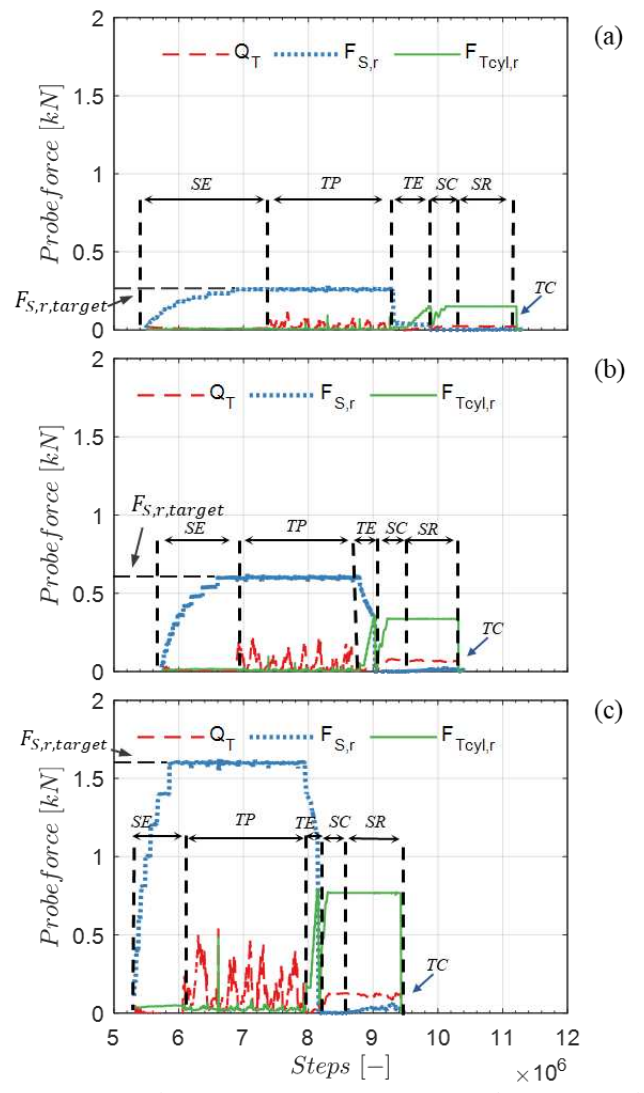


Figure 5. Evolution of representative forces during one self-burrowing cycle under (a) 1/6g, (b) 1/3g and (c) 1g gravity condition.

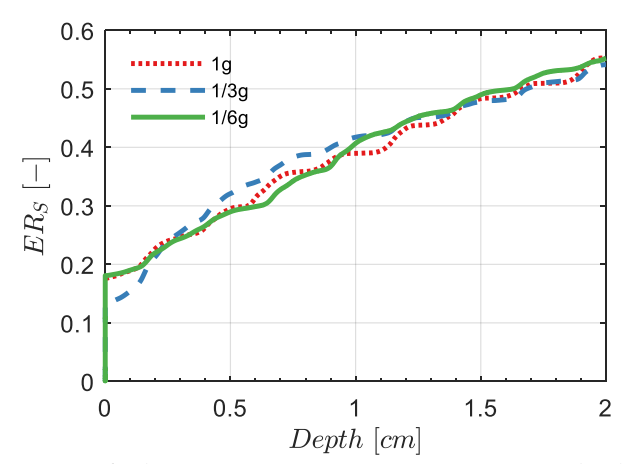


Figure 6. Shaft expansion ratio ERs vs penetration depth

# 3.3 Work done during all self-burrowing steps

The work done by each of the steps was calculated to quantify the energy consumption of the burrowing behaviours. Figure 7 shows the effects of gravity on the total work done by the self-burrowing behaviours ( $W_{tot}$ ) and the two main work components done by tip oscillation ( $W_{TO}$ ) and shaft expansion ( $W_{SE}$ ). Gravity conditions present an almost linear relationship with  $W_{tot}$ ,  $W_{TO}$ , and  $W_{SE}$ . The tip resistance reduction method – tip oscillation – consumes most of the required total work, namely, 63% - 67%, while shaft expansion consumes 25% - 29% of the total work.

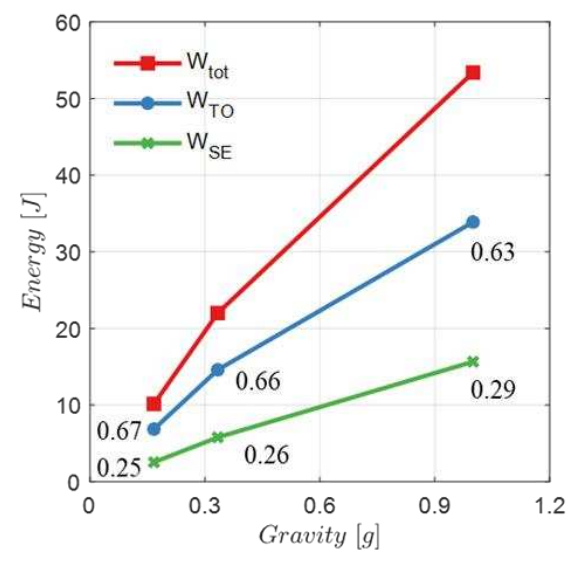


Figure 7. Work components calculated during one self-burrowing cycle vs gravity.

# 4 DISCUSSION

As presented in section 3.2, the shaft radial force  $F_{S,r}$  drops suddenly to a low value, affected by tip expansion. It was not clear whether the sudden change was caused by residual shaft expansion velocity from TPO or by the subsequent TE.

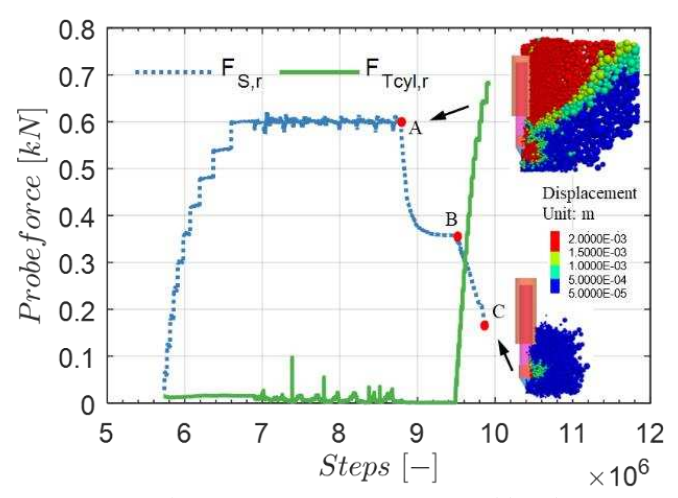


Figure 8. Exploration of reasons for  $F_{S,r}$  sudden decrease in TE using the 1/3g sample

To explore the reasons, we first equilibrate the system by setting the residual shaft expansion velocity to zero in the 1/3g sample. At this stage,  $F_{S,r}$  decreases from point A until reaching a plateau value at point B, as shown in Figure 8. At point A, large particle displacements mainly concentrate around the shaft. The displacement accumulation was cleared to 0 at point B to better visualize the tip expansion effect on particle displacement. After equilibrating the system (point B), the tip starts to expand to reach its target force. During this stage, it is observed that  $F_{S,r}$  continues the decrease to point C, indicating an interactive effect between the tip expansion and the shaft force evolution. The interaction is reflected from the particle displacement contour at point C, i.e., particles around the shaft move away with tip expansion causing the decrease of  $F_{S,r}$ .

From above analyses, we can conclude that the sudden decrease of  $F_{S,r}$  during TE is resulted from the combination of residual shaft expansion velocity and tip expansion.

#### 5 CONCLUSIONS

This study has explored the feasibility of the operation of a bio-inspired self-burrowing probe in soils with various low gravity level, namely, 1/6g, 1/3g, and 1g. The self-burrowing process consists of six individual steps: shaft expansion, tip penetration with oscillation, tip expansion, shaft contraction, shaft retraction, and tip contraction. It is shown that the burrowing could achieve an equal distance of 2 cm, regardless of the gravity level. Energy required to complete one self-burrowing cycle increases almost linearly with gravity, and tip oscillation consumes more than 50% of the total energy. The sudden drop of shaft radial force during tip expansion is caused by both residual shaft expansion velocity and tip expansion behaviour. The findings in this study could suggest that the probe can potentially be used for soil testing and sensor deployment on outer-space bodies such as the Mars and the Moon. Soil samples with

higher gs are expected to run to cover a wider range of gravity level.

#### 6 ACKNOWLEDGEMENTS

The first author has received support from a CSC grant, which is greatly acknowledged. The second author thanks the financial support of the Theodore von Kármán Fellowship - outgoings 2023 (GSO082) from RWTH Aachen University. This material is based upon work supported in part by the Engineering Research Center Program of the National Science Foundation under NSF Cooperative Agreement No. EEC–1449501. Any opinions, findings, and conclusions or recommendations expressed in this material are those of the author(s) and do not necessarily reflect those of the National Science Foundation.

# 7 REFERENCES

Dorgan, K.M., 2015. The biomechanics of burrowing and boring. *Journal of Experimental Biology*, 218(2), pp.176-183.

Germann, D.P., Schatz, W. and Hotz, P.E., 2011. Artificial bivalves—the biomimetics of underwater burrowing. *Procedia Computer Science*, 7, pp.169-172.

Huang, S. and Tao, J., 2020. Modeling clam-inspired burrowing in dry sand using cavity expansion theory and DEM. *Acta Geotechnica*, 15(8), pp.2305-2326.

Itasca, C. G. I. 2017. PFC — Particle Flow Code, Ver. 5.0. Minneapolis.

Jiang, M., Liu, F., Wang, H., Wang, X. 2015. Investigation of the effect of different gravity conditions on penetration mechanisms by the distinct element method. *Engineering Computations*, 32(7), 2067-2099.

Mahaffy, Paul R., Christopher R. Webster, Michel Cabane, Pamela G. Conrad, Patrice Coll, Sushil K. Atreya, Robert Arvey et al. 2012. The sample analysis at Mars investigation and instrument suite. *Space Science Reviews* 170: 401-478.

Trueman, E.R., 1967. The dynamics of burrowing in Ensis (Bivalvia). *Proceedings of the Royal Society of London. Series B. Biological Sciences*, 166(1005), pp.459-476.

Wei, H., Zhang, Y., Zhang, T., Guan, Y., Xu, K., Ding, X. Pang, Y., 2021. Review on bioinspired planetary regolith-burrowing robots. *Space Science Reviews*, 217, pp.1-39.

Winter, V., Deits, R. L. H., Dorsch, D. S., Slocum, A. H., & Hosoi, A. E. 2014. Razor clam to RoboClam: Burrowing drag reduction mechanisms and their robotic adaptation. *Bioinspiration and Biomimetics*, 9(3).

Zhang, N., Ciantia, M. O., Arroyo, M., & Gens, A. 2021. A contact model for rough crushable sand. *Soils and Foundations*, 61(3), 798–814.

Zhang, N., Chen, Y., Martinez, A., Fuentes, R. 2023. DEM Simulation of a Bio-Inspired Self-Burrowing Probe in Granular Materials. *GeoCongress* 2023. (accepted)

Zhang, T., Xu, K., Yao, Z., Ding, X., Zhao, Z., Hou, X., Pang, Y., Lai, X., Zhang, W., Liu, S. and Deng, J., 2019. The progress of extraterrestrial regolith-sampling robots. *Nature Astronomy*, 3(6), pp.487-497.